
Masked Diffusion Models Are Fast and Privacy-Aware Learners

Jiachen Lei Peng Cheng Zhongjie Ba * Kui Ren

School of Cyber Science and Technology
Zhejiang University

Abstract

Diffusion models have emerged as the *de-facto* technique for image generation, yet they entail significant computational overhead, hindering the technique’s broader application in the research community. We propose a prior-based denoising training framework, the first to incorporate the pre-train and fine-tune paradigm into the diffusion model training process, which substantially improves training efficiency and shows potential in facilitating various downstream tasks. Our approach centers on masking a high proportion (e.g., up to 90%) of the input image and employing masked denoising score matching to denoise the visible areas, thereby guiding the diffusion model to learn more salient features from training data as prior knowledge. By utilizing masked learning in a pre-training stage, we efficiently train the ViT-based diffusion model on CelebA-HQ 256×256 in the pixel space, achieving a 4x acceleration and enhancing the quality of generated images compared to denoising diffusion probabilistic model (DDPM). Moreover, our masked pre-training technique can be universally applied to various diffusion models that directly generate images in the pixel space, aiding in the learning of pre-trained models with superior generalizability. For instance, a diffusion model pre-trained on VGGFace2 attains a 46% quality improvement through fine-tuning with merely 10% data from a different distribution. Moreover, our method shows the potential to serve as a training paradigm for enhancing the privacy protection capabilities of diffusion models. Our code is available at <https://github.com/jiachenlei/maskdm>.

1 Introduction

Diffusion models or score-based generative models [61, 60, 28, 56, 35, 16] have emerged as the state-of-the-art technique in generative modeling, exhibiting remarkable performance in image synthesis. The denoising training, the core of the diffusion-based approach, has been quickly adopted in various domains such as image editing[51, 21, 2, 55], controllable image generation[46, 45, 52, 18, 44, 50, 13, 3], video synthesis[5, 30], and audio generation[65, 37]. These advancements have significantly contributed to the progress of generative modeling since the advent of generative adversarial networks (GAN)[22, 1, 53, 24], and diffusion models are taking over the predominating role of GAN-based methods[32, 34].

Although diffusion models demonstrate exceptional capability in image synthesis, they require intensive computational resources. As one type of likelihood-based generative model, diffusion models demonstrate strong mode-covering ability [48], which unfortunately makes them pay excessive attention to model the details of images. Consequently, these models require more training effort, particularly when dealing with high-resolution images [28]. While large-scale diffusion models such as Stable Diffusion[48] and DALL·E 2 [45] have achieved impressive results in high-resolution image

*Corresponding author

synthesis, the significant computational resources and training overhead required for these models are affordable only to large organizations, severely prohibiting the accessibility of these generative technologies to broader research communities and audiences.

To alleviate the overall training expenses associated with diffusion models when trained on high-resolution images, we propose **Prior-Based Denoising Training**, a novel training framework incorporating prior learning into the denoising training process. Rather than directly approximating the target data distribution, we decompose the denoising process into two simple yet related training stages, creating a smooth and sequential learning path for diffusion models: the first stage, *masked pre-training*, masks parts of the input image and performs **Masked Denoising Score Matching (MDSM)** on the visible parts, followed by *denoising fine-tuning* equipped with the conventional denoising score matching (DSM) objective [28, 63] as the second stage. Our key observation is that, when optimized through MDSM, the model initially endeavors to approximate prominent features in the training data (such as the fundamental characteristics of a human face), thereby directing less attention toward subtle features, which exhibit considerable variability, and implicitly capturing prior knowledge of the distribution. In subsequent DSM, the model learns to capture more informative details and approximates training data distribution more stably and expeditiously. Finally, the standard sampling process [61] can be applied to the trained model for image synthesis.

Our two-stage prior-based learning framework achieves substantial efficiency improvement in the training process. Utilizing the framework, diffusion model training poses significantly less time overhead. Meanwhile, the trained models can generate high-quality images comparable to state-of-the-art methods. We demonstrate that our method could achieve approximately **4x acceleration** on convergence speed in comparison to DDPM [28] on CelebA-HQ 256×256 .

In addition to reducing the training cost, the proposed framework exhibits other advantages. Firstly, the proposed masked pre-training is a plug-and-play technique that can be combined with arbitrary denoising training algorithms. In this paper, we conduct experiments with vision transformer (ViT) [17] based network, UViT [4], within the context of DDPM. Still, our two-stage training framework can flexibly accelerate the denoising process for various diffusion model variants, e.g., diffusion models with CNN-based UNet [49] architectures or other denoising training frameworks [61, 60]. Secondly, the pre-trained model obtained from masked pre-training demonstrates excellent generalizability, benefiting a range of downstream tasks: 1) it efficiently reduces model training expenses in various downstream tasks; 2) it aids in fine-tuning diffusion models when facing limited training data. Lastly, in privacy-sensitive applications, the pre-trained models represent a lower risk of exposing training data due to the masking strategy, which moderates the leakage of private information (e.g., human faces).

The **contributions** of our work can be summarized as follows:

- (i) To the best of our knowledge, we are the first to propose a prior-based denoising training framework that significantly reduces the cost of diffusion model training.
- (ii) We propose to incorporate pre-training and fine-tuning paradigms into the diffusion model training. In particular, we incorporate the masking strategy into the pre-training stage, forcing the diffusion model to learn prominent features from data. The pre-trained model expedites the following fine-tuning significantly and exhibits good generalizability for facilitating downstream tasks with limited data. In addition, we present a theoretical explanation of why masked training exhibits such advantages.
- (iii) Our approach, compatible with arbitrary diffusion-based algorithms and network architecture, supports high-resolution image synthesis beyond the latent space. We conduct experiments to train ViT-based diffusion models using CelebA-HQ 256×256 in the pixel space, reducing the training cost to merely 25% of the baseline DDPM [28] while achieving better image generation. Moreover, our pre-trained model demonstrates excellent generalizability: fine-tuning the pre-trained model with only 10% of local data shows an improvement of 46% in the performance metric for the downstream task.
- (iv) We demonstrate that integrating masking into diffusion training within the pixel space can reduce privacy leakage from the training data. Moreover, it can mitigate the pre-trained model’s ability for memorizing and regenerating training data, reducing the risk of sensitive information extraction from training data.

2 Preliminary on Diffusion Models

Diffusion Models [56, 28] are latent variable models and are composed of a forward and a reverse process. The forward process is defined as a discrete Markov chain of length T : $q(\mathbf{x}_{1:T}|\mathbf{x}_0) = \prod_{t=1}^T q(\mathbf{x}_t|\mathbf{x}_{t-1})$. For each step $t \in [1, T]$ in the forward process, a diffusion model adds noise ϵ_t sampled from the standard Gaussian distribution $N(0, I)$ to data \mathbf{x}_{t-1} and obtains disturbed data \mathbf{x}_t from $q(\mathbf{x}_t|\mathbf{x}_{t-1}) = \mathcal{N}(\mathbf{x}_t; \sqrt{1 - \beta_t}\mathbf{x}_{t-1}, \beta_t\mathbf{I})$. β determines the scale of added noise at each step and is prescribed such that $p(\mathbf{x}_T) \approx N(0, I)$.

Ho et al. [28] propose to use untrained linear β schedule where β_t increases linearly in the range of $[10^{-4}, 0.02]$. Later, Nichol et al. [40] introduce the cosine schedule to mitigate abrupt changes in noise level at $t = 0$ and $t = T$. Empirical evidence demonstrates that adopting the cosine schedule improves both the Negative Log-likelihood (NLL) and the sample quality of the diffusion model. Noticeably, instead of sampling sequentially along the Markov chain, we can sample x_t at any time step t in the closed form via $q(\mathbf{x}_t|\mathbf{x}_0) = N(\mathbf{x}_t; \sqrt{\bar{\alpha}_t}\mathbf{x}_0, (1 - \bar{\alpha}_t)I)$, where $\bar{\alpha}_t = \prod_{s=1}^t (1 - \beta_s)$.

The reverse process is also defined as a Markov chain: $p_\theta(\mathbf{x}_{0:T}) = p(\mathbf{x}_T) \prod_{t=1}^T p_\theta(\mathbf{x}_{t-1}|\mathbf{x}_t)$. In [28], $p_\theta(\mathbf{x}_{t-1}|\mathbf{x}_t)$ is parameterized as $N(\mathbf{x}_t; \mu_\theta(\mathbf{x}_t, t), \sigma_t)$, where $\mu_\theta(\mathbf{x}_t, t) = \frac{1}{\sqrt{\alpha_t}}(\mathbf{x}_t - \frac{\beta_t}{\sqrt{1-\bar{\alpha}_t}}\epsilon_\theta(\mathbf{x}_t, t))$ and σ_t is time dependent constant. ϵ_θ is parameterized by a neural network of which inputs are \mathbf{x}_t and time step t . Using this parameterization, the objective in [56] is simplified to:

$$L_{simple}(\theta) = \mathbb{E}_{t, \mathbf{x}_0, \epsilon} \left[\left\| \epsilon - \epsilon_\theta(\sqrt{\bar{\alpha}_t}\mathbf{x}_0 + \sqrt{1 - \bar{\alpha}_t}\epsilon, t) \right\|^2 \right] \quad (1)$$

As discussed in [61], the objective described in Eq.1 is essentially denoising score matching [63] and is the discretization of a particular continuous stochastic differential equation.

Subsequent to the training, samples are generated via iterating through the reverse process $p_\theta(\mathbf{x}_{0:T})$. Specifically, \mathbf{x}_T is first sampled from a standard Gaussian distribution $\mathcal{N}(0, \mathbf{I})$ and \mathbf{x}_t in each step is predicted as follows, where \mathbf{z} is sampled from a standard Gaussian distribution $\mathcal{N}(0, \mathbf{I})$.

$$\mathbf{x}_{t-1} = \frac{1}{\sqrt{\alpha_t}} \left(\mathbf{x}_t - \frac{1 - \alpha_t}{\sqrt{1 - \alpha_t}} \epsilon_\theta(\mathbf{x}_t, t) \right) + \sigma_t \mathbf{z} \quad (2)$$

3 Prior-based Denoising Training

3.1 Key Insight

Our idea is inspired by the observation of the relationship between marginal and joint distribution. Consider an image denoted by $\mathbf{x}_0 = (x_0^1, x_0^2, x_0^3, \dots, x_0^N)^2$, where $\mathbf{x}_0 \in R^N$, and N represents the number of image pixels. Given a dataset of distribution $p(\mathbf{x}_0)$, which can be expressed as the joint distribution of N pixels, $p(\mathbf{x}_0) = p(x_0^1, x_0^2, x_0^3, \dots, x_0^N)$, our objective is to approximate the data distribution with $p_\theta(\mathbf{x}_0)$. Let τ represents a randomly selected subsequence of $[1, \dots, N]$ with a length of S . The marginal distribution of pixels, determined by τ , can be expressed as $p(\{x_0^{\tau_i}\}_{i=1}^S) = p(x_0^{\tau_1}, x_0^{\tau_2}, x_0^{\tau_3}, \dots, x_0^{\tau_S})$.

It is important to highlight that the distribution $p(\mathbf{x}_0)$ belongs to a family \mathcal{Q} of distributions that share the same set of $\binom{N}{S}$ possible marginal distributions $p(\{x_0^{\tau_i}\}_{i=1}^S)$. We introduce the term "marginal proxy distribution" to refer to any distribution in \mathcal{Q} other than $p(\mathbf{x}_0)$ that satisfies this condition. We represent such distributions using the notation $p_{\phi_S}(\mathbf{x}_0)$, where ϕ represents the parameters of the distribution and S specifies the length of the subsequence τ . Intuitively, the parameter S determines the degree of average similarity between the true data distribution and its marginal proxy distributions such that a higher value of S indicates a greater resemblance.

We demonstrate an example in the two-dimensional space. Assuming that we are approximating the Swiss roll distribution $p(\mathbf{x}_0)$, where $\mathbf{x}_0 = (x_0, y_0)$, Fig.1 displays a concrete example of the marginal proxy distribution $p_{\phi_1}(\mathbf{x}_0)$ in a blue heatmap which fully covers the Swiss roll data distribution (represented by the red line). Here, $S = 1$ implies that only a single component, x_0 or y_0 , is taken in a marginal distribution. $p_{\phi_1}(\mathbf{x}_0)$ shares the same marginal distribution $p(x_0)$ and $p(y_0)$ as the Swiss roll data while assuming independence between x_0 and y_0 such that $p_{\phi_1}(\mathbf{x}_0) = p(x_0)p(y_0)$.

²We follow the conventions and denote a clean image as \mathbf{x}_0 , where the subscript 0 is the time step.

It is worth noting that there also exist other instances of $p_{\phi_1}(\mathbf{x}_0)$ that do not assume independence between x_0 and y_0 .

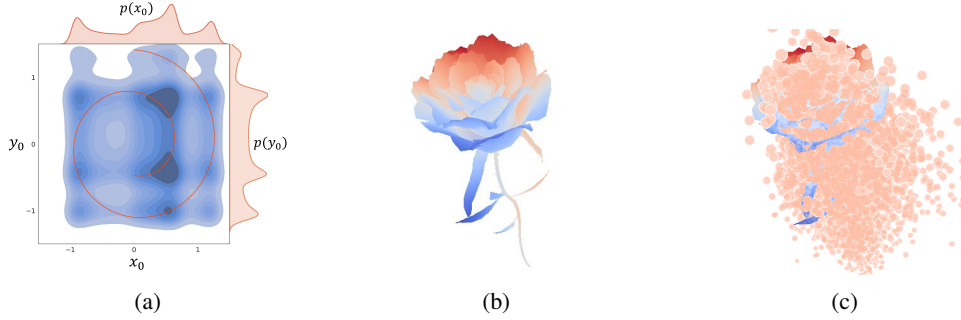


Figure 1: Toy example. (a) a 2D Swiss roll approximation example, where the red line is the Swiss roll distribution, the blue heatmap in the background is an instance of distribution $p_{\phi_1}(\mathbf{x}_0)$, and the top and right curve denote marginal distribution $p(x_0)$ and $p(y_0)$. (b) a 3D "rose" shape approximation example. (c) the rose is closely surrounded by 10k points that are sampled from the learned distribution $p_{\phi_2}(\mathbf{x}_0)$

When fitting either $p(x_0)$ or $p(y_0)$, both of which can be seen as multi-modal Gaussian distributions, we observe that approximating $p_{\phi_1}(\mathbf{x}_0)$ is comparatively easier than modeling the Swiss roll distribution $p(\mathbf{x}_0)$. Moreover, by leveraging the prior knowledge from $p_{\phi_1}(\mathbf{x}_0)$, we can efficiently approximate the true Swiss roll distribution instead of beginning from scratch. This is because $p_{\phi_1}(\mathbf{x}_0)$ fully covers the Swiss roll distribution, with the curve traversing most of its modes.

3.2 Overview

Motivated by the observations, we propose Prior-Based Denoising Training, which comprises two stages to approximate the data distribution $p(\mathbf{x}_0)$. In the first *masked pre-training* stage, we perform masked denoising score matching to learn a marginal proxy distribution $p_{\phi_S}(\mathbf{x}_0)$ from the distribution family \mathcal{Q} that "encompasses" the true distribution. Since S is the important hyperparameter and the specific form of $p_{\phi_S}(\mathbf{x}_0)$ is not crucial for the training process, we implicitly approximate certain instances of $p_{\phi_S}(\mathbf{x}_0)$ by learning all possible marginal distributions $p(\{x_0^{\tau_i}\}_{i=1}^S)$ based on a randomly initialized neural network. In the second *denoising fine-tuning* stage, based on the learned prior $p_{\phi_S}(\mathbf{x}_0)$ from the first stage, we continue to estimate $p(\mathbf{x}_0)$ via the objective in Eq.1.

3.3 Masked Pre-training and Sampling

In this section, we formulate the objective function (i.e., MDSM) in the masked pre-training, demonstrate the first stage's training process, and further illustrate the sampling process of a model trained with our two-stage framework. We skip the introduction of the denoising fine-tuning since it is the same as the conventional denoising training process (see Section 2).

We approximate $p_{\phi_S}(\mathbf{x}_0)$ using a conditional diffusion model $p_{\theta}(\mathbf{x}_0|\tau)$, where the subsequence of pixels $\{x_0^{\tau_i}\}_{i=1}^S$ input into the model or the target marginal distribution is specified by τ . To achieve this, we employ a masking operation where we incorporate a randomly sampled sparse matrix $\mathbf{M} \in \{0, 1\}^{N \times N}$ and $\sum_{i=0}^N \mathbf{M}_{ij} = 1$, $\sum_{i,j} \mathbf{M}_{ij} = S$. As shown in Eq.3, this masking operation allows us to arbitrarily sample a subsequence $\{x_0^{\tau_i}\}_{i=1}^S$ from \mathbf{x}_0 .

$$\hat{\mathbf{x}}_0 = (\mathbf{x}_0 + \mathbf{H}) \cdot \mathbf{M} = \mathbf{x}_0 \cdot \mathbf{M} + \mathbf{H} \cdot \mathbf{M} \quad (3)$$

where $\mathbf{H} \in R^N$ can be represented as $\mathbf{H} = (h_1, h_2, \dots, h_N)$, and $\hat{\mathbf{x}}_0 = (x_0^{\tau_1} + h_{\tau_1}, x_0^{\tau_2} + h_{\tau_2}, x_0^{\tau_3} + h_{\tau_3}, \dots, x_0^{\tau_S} + h_{\tau_S})$. Each element of \mathbf{H} encodes the property (e.g., position) of the corresponding pixel x , which is known as positional embedding in vision transformer family[17, 38]. In this way, different combinations of pixels, specified by τ , are implicitly encoded in the corresponding subset of \mathbf{H} , allowing for the representation of possible marginal distributions. Meanwhile, the conditional model $p_{\theta}(\mathbf{x}_0|\tau)$ is converted into an unconditional one, $p_{\theta}(\hat{\mathbf{x}}_0)$, with the condition τ being merged

with the model input. Consequently, the sampling of \mathbf{x}_t at any given time step can be expressed as: $\hat{\mathbf{x}}_t = \sqrt{\bar{\alpha}_t}\hat{\mathbf{x}}_0 + \sqrt{1 - \bar{\alpha}_t}\epsilon$. We optimize the following MDSM objective:

$$L_{mdsm}(\theta) = \mathbb{E}_{t, \hat{\mathbf{x}}_0, \epsilon} \left[\|\epsilon - \epsilon_\theta(\sqrt{\bar{\alpha}_t}\hat{\mathbf{x}}_0 + \sqrt{1 - \bar{\alpha}_t}\epsilon, t)\|^2 \right] \quad (4)$$

The objective is formulated in a manner that exposes more similarity to the one used in Eq.1. Our method is agnostic to specific model architectures and we demonstrate the training together with sampling pipeline using a ViT-based backbone (see Fig.2 for illustration).

Training. Given an image $\mathbf{x}_0 \sim p(\mathbf{x}_0)$, our first step is to partition it into non-overlapping patches of size $p \times p$. Subsequently, we perform the masking operation in Eq.3 to all patches, retaining only visible ones, denoted as $\hat{\mathbf{x}}_0$. The visible patches are linearly mapped into tokens before element-wisely added with positional embedding. The number of visible patches, S , is predetermined and fixed throughout the training process. For clarity, we use mask rate m in place of parameter S , formulated as $m = 1 - \frac{S}{N}$. We will present further analysis on the influence of mask rate and the selection of M in Section 4.2. The final step involves masked denoising score matching on the visible patches to approximate the set of all possible distributions $p(\hat{\mathbf{x}}_0)$.

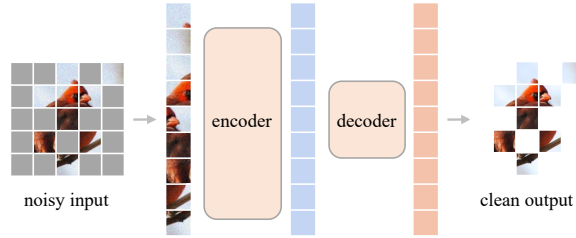


Figure 2: Illustration of the overall training process of masked diffusion model.

Sampling. We sample from $p_\theta(\hat{\mathbf{x}}_0)$ by setting M as 1. Thereafter, following the procedure of DDPM in Eq.2, the sampling step is:

$$\hat{\mathbf{x}}_{t-1} = \frac{1}{\sqrt{\alpha_t}} \left(\hat{\mathbf{x}}_t - \frac{1 - \alpha_t}{\sqrt{1 - \alpha_t}} \epsilon_\theta(\hat{\mathbf{x}}_t, t) \right) + \sigma_t \mathbf{z} \quad (5)$$

In the context of 3-dimensional space, we present an example featuring an intricate target distribution resembling a rose flower. To effectively capture this distribution, we initially choose $S = 2$ and estimate the two-dimensional marginal distributions of the target distribution via MDSM, specifically $p(x_0, y_0)$, $p(x_0, z_0)$, and $p(y_0, z_0)$. As shown in Fig.1, we observe that a learned marginal proxy distribution $p_{\phi_2}(\mathbf{x}_0) = p(x_0, y_0, z_0)$, fully encompasses the rose flower distribution. Leveraging the learned marginal prior $p_{\phi_2}(\mathbf{x}_0)$ as a favorable starting point, the model rapidly captures the actual distribution.

4 Experiments

4.1 Experimental Setup

Datasets. We mainly conduct experiments on three datasets: CelebA [39], CelebA-HQ [34] and VGGFace2 [7]. Images from these datasets are resized and center cropped into 64×64 , 256×256 , and 256×256 , respectively, with each image’s aspect ratio remains unchanged.

Model configurations. In our experiments, we employ three model configurations, with the parameter count ranging from 44 M to 233 M. These architectures are based on the U-ViT models proposed in [4], with certain modifications. In all configurations, we adopt a single linear layer as the decoder and discard the convolutional block initially appearing in the U-ViT model. Further details regarding the configurations can be found in Table 4.

Implementation details. Similar to the settings in [4], we conduct all experiments with mixed precision considering training efficiency and employ the AdamW optimizer with coefficients set to (0.99, 0.99). The maximum diffusion steps T is set to 1000. We maintain an exponential moving average (EMA) model during training and use the EMA model during sampling. Due to limited

computing resources, we perform discrete wavelet transformation (DWT) in our unconditional image synthesis experiments to decompose the training images of CelebA-HQ, which is also applied to the baseline model for a fair comparison. Further detailed information is provided in the Appendix 5.

Evaluation Settings. During the evaluation, we employ DDIM [58] to generate samples and present the FID-N score calculated between the generated samples and the entire training set. Fréchet Inception Distance (FID) [27] is the prevailing metric for measuring image quality, and the N in FID-N indicates the total number of generated images used for FID score computation.

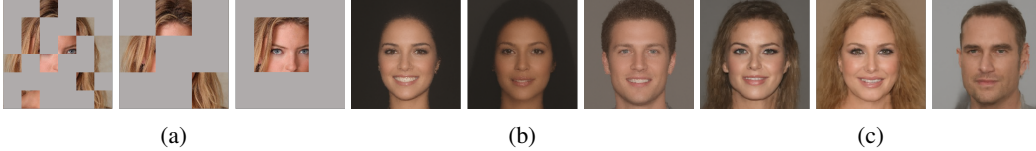


Figure 3: (a) Three mask sampling strategies are examined in our experiments. From left to right, the strategies are represented as patch-wise masking, block-wise masking, and cropping. Samples in (b) and (c) are generated via MaskDM-B pre-trained on CelebA-HQ 256×256 , equipped with 90% patch-wise and block-wise masking, respectively. Notably, the model pre-trained with cropping at a 90% mask rate exhibits limited capability in generating plausible samples; therefore, we do not illustrate the results.

4.2 Optimal Mask Rate and Type: An Investigation

Mask	FID↓	Mask	FID↓	Mask	FID↓	Mask	Ratio	#Steps	FID↓
scratch	7.55	cropping	6.82	cropping	8.62	2x2 block	50%	100k	6.27
cropping	6.92	patch	6.58	patch	7.34	2x2 block	50%	150k	6.05
patch	6.85	2x2 block	6.51	2x2 block	8.99	patch (2xBS)	10%	50k	6.31
2x2 block	6.77	4x4 block	6.88	4x4 block	6.91	2x2 block (2xBS)	10%	50k	6.71
4x4 block	6.92	8x8 block	7.43						

(a) Mask ratio: **10%** (b) Mask ratio: **50%** (c) Mask ratio: **90%** (d) Impact of training overhead.

Table 1: **Fine-tuning experiments** on CelebA 64×64 , where pre-trained weights are acquired from different masking configurations. The FID score is computed on 10k samples. The notation ‘2xBS’ indicates that the batch size used is twice the default size under the given masking setting. #Steps denotes pre-training steps. The baseline model, trained from scratch without loading any weights, is marked in gray.

Pre-training settings. We mainly adopt patch-wise masking, block-wise masking, and cropping to generate the mask vector M discussed in Eq.3. The manifestation of each mask type is shown in Fig.3a: patch-wise masking entails the random occlusion of a predefined number of image patches. Block-wise masking involves randomly selecting image blocks for masking, where each block comprises a fixed quantity of image patches. Lastly, cropping entails randomly selecting a square region by determining its top-left coordinates and masking the area outside the chosen square. Models are then trained, on CelebA 64×64 , using these techniques at mask ratios of 10%, 50%, and 90%, respectively. During pre-training, the training overhead regarding GPU memory usage is fixed across different experiments and the default training step is set as 50k iterations.

Fine-tuning. In the investigation of optimal mask configurations, we fine-tune models pre-trained with the above-mentioned mask strategies and compare their performances. We perform this fine-tuning for 200k steps employing the conventional denoising objective delineated in Eq. 1. In the interest of a fair comparison, we include a baseline model that undergoes training from scratch for 250k steps, ensuring that the total training time is comparable to models with pre-loaded weights.

As shown in Tab.1, the model pre-trained at 50% mask ratio outperforms other counterparts in most cases. The model, with 50% 2x2 block-wise masked pre-training, attains an impressive FID score of 6.51, significantly exceeding the baseline score while exhibiting faster convergence speed. Based on the empirical results, the mask ratio is critical in optimizing the advantages of masked pre-training, and selecting an appropriate mask type is also crucial in determining the final model’s performance.

Masking Strategies and Computing Overhead. Different mask strategies pose various requirements on computing resources. We evaluate our approach’s performance by considering both masking strategies and computing overhead to provide a practical perspective of our training framework.

Compared to higher mask rates, training a model with a lower mask ratio renders a smaller batch size because of limited GPU memory. If GPU constraints are alleviated to achieve the same batch size, training with lower mask rates requires more time due to increased visible areas, assuming we keep the training steps the same as the higher mask rate cases. Consequently, we manually double the pre-training batch size for low-ratio masking and extend the number of pre-training steps for high-ratio masking to assess the performance changes given various computing resources. The results are presented in Tab.1d. As anticipated, models exhibit better performance with sufficient training resources. Specifically, the model pre-trained with 10% patch-wise masking significantly boosts the FID score, reaching 6.31. The 50% 2x2 block-wise masking configuration, with increased training steps, also demonstrates substantial performance growth, obtaining an FID score of 6.27. This is achieved with a training duration similar to 10% patch-wise masking.

We find the models, pre-trained with a 90% mask ratio, exhibit a rapid divergence in FID score after 50k training steps. We delve deeper into the root causes of this training instability by studying various impact factors, with the detailed findings presented in Appendix D.1. Experimental outcomes confirm that the noise schedule is a significant factor impacting training stability among the hyperparameters. Consequently, we opt for a cosine noise schedule[40] in the ensuing sections.

In summary, it is crucial to select a mask rate that optimizes training efficiency and aligns with affordable computing resources. Training with a lower mask rate requires more GPU resources despite offering faster convergence speed in fine-tuning, given the same hyperparameters (e.g., batch size and training steps) as pre-training at higher mask rates. For instance, experiments using a 10% mask ratio consume $1.5\times$ more GPU than those using a 50% mask ratio, and this cost increases quadratically with image data resolution. On the other hand, a higher mask ratio requires fewer computing resources (i.e., GPUs) but slightly increases time costs to achieve performance comparable to its lower mask ratio counterparts. Notably, a 90% mask rate for processing datasets like CelebA 64×64 might cause optimization issues and high IO load due to the large batch size resulting from extensive masking.

4.3 Unconditional Image Synthesis

We conduct unconditional image synthesis experiments on CelebA-HQ 256×256 using masked pre-training to train two models: MaskDM-B and MaskDM-L. For comparative purposes, we also train a baseline model using the objective detailed in Eq. 1, with identical hyperparameter settings as those utilized in the fine-tuning stage of the pre-trained MaskDM-L model.

Training acceleration. As illustrated in Fig.4, incorporating masked pre-training significantly enhances the performance of the vanilla DDPM. Building upon the pre-trained weights, the MaskDM-L model attains an FID score of nearly 20 in a mere 10k steps in denoising fine-tuning. Moreover, we significantly reduce the associated training costs compared to the baseline. Our approach attains an approximate $4\times$ **speedup** during the fine-tuning phase. We anticipate the acceleration effect to be further enhanced as the dimensionality of the data in the target distribution increases.

Performance comparison. We proceed to compare our approach with state-of-the-art diffusion-based image synthesis approaches, utilizing the FID scores reported in corresponding papers as their performance measurement. At present, there is a lack of research employing diffusion models with ViT-based architecture for high-dimensional image synthesis beyond latent space. To the best of our knowledge, GenViT[66] is the solitary work in this field. The scarcity of studies stems from the training challenges associated with the lack of inductive bias in the ViT and the computation complexity of the attention mechanism [19].

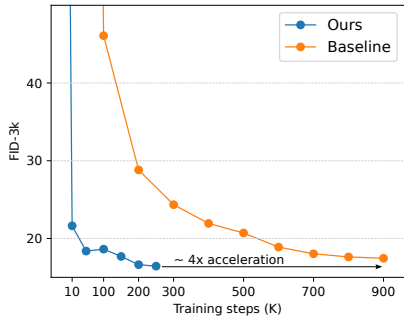


Figure 4: FID-3k vs. training steps

As shown in Tab.2, Gen-ViT [66] achieves FID of 22.07 on CelebA-HQ 128×128 , which underscores the challenges of training a ViT-based diffusion model to generate high-dimensional images. Additionally, it is notable that the number of Gen-ViT’s parameters is a mere 12.9 M, reflecting the difficulty associated with model parameter scaling that requires substantial computational resources such as GPU units. Regarding synthesizing 256×256 images, our MaskDM-B model attains an FID score of 10.77, outperforming DiffuseVAE[41] with fewer parameters. Moreover, our MaskDM-L achieves an FID score of 9.67 after 23 V100-day fine-tuning. This performance significantly exceeds the baseline model, which necessitates 38.3 V100-days of training, while concurrently demanding less training costs.

Our **primary goal** is not to obtain a new state-of-the-art performance but rather to achieve efficient training of diffusion models through masked pre-training. As such, our focus is not on achieving the optimal FID performance, thereby reducing the emphasis on pursuing a high FID score once satisfactory results are obtained. Nonetheless, it is viable to further enhance this metric using sophisticated denoising training methods [35, 31].

Method	FID-30k ↓	Params	Cost ↓
VQ-GAN[19]	10.2	355M	-
TransGAN[33]	9.6	-	92.8
WaveDiff* [43]	5.94	31.48M	4.84
LSGM [62]	7.22	-	-
LDM-4[48]	5.11	274M	14.4
Gen-ViT** [66]	22.07	12.9M	-
DiffuseVAE [41]	11.28	146M	-
Baseline	12.06	233M	38.3
MaskDM-B	10.77	102M	24.3
MaskDM-L	9.67	233M	23

Table 2: Qualitative analysis on CelebA-HQ. * indicates that the model training cost is converted into V100-day as done in [48]. ** indicates that the model is trained and evaluated on the image resolution of 128×128 .

4.4 Generalizability

In addition to presenting an efficient training approach for image synthesis, we aim to provide a pre-trained model facilitating seamless fine-tuning for diverse downstream tasks. To assess the feasibility, we investigate the generalizability of the pre-trained model. Our evaluation considers practical scenarios in real-world applications, accounting for data distribution shifts and varying amounts of data between the pre-training and downstream fine-tuning (i.e., the amount of local training data for downstream tasks is smaller).

We construct local training datasets comprising 10% and 1% of the CelebA-HQ 256×256 images and evaluate the performance of three models trained under distinct configurations. The baseline model employs the objective in Eq.1 and is trained from scratch on the limited data. In contrast, the other two models leverage weights pre-trained with 90% mask, on the complete CelebA-HQ 256×256 and VGGFace2 256×256 datasets, respectively.

Training data	Baseline	Pre-trained on CelebA-HQ	Pre-trained on VGGFace2
10% data	37.17	24.59 (34% ↓)	20.71 (46% ↓)
1% data	63.33	32.51 (49% ↓)	36.51 (42% ↓)

Table 3: FID of different models, trained under different settings. Utilizing the **complete** CelebA-HQ 256×256 dataset as a reference, the FID score is computed on 10k samples.

As demonstrated in Tab.3, masked pre-training can significantly enhance diffusion models’ performance. When only 10% of local data is accessible for training, the model pre-trained on the VGGFace2 256×256 dataset yields the best performance, exhibiting a 46% reduction in FID score compared to the baseline model. Meanwhile, the distribution approximated by the model pre-trained on CelebA-HQ 256×256 bears the highest resemblance to the 1% CelebA-HQ data distribution, achieving a 49% decrease in FID score. This finding suggests that a similar pre-training dataset is more advantageous when the available local training data is extremely limited.

4.5 Privacy Preserving

Diffusion models tend to memorize training data and regenerate them at generation time, causing privacy-violating consequences [9]. Therefore, there is an urgent need for effective solutions that can preserve privacy during the training of image diffusion models. Our prior-based diffusion training can be treated as a promising initiation in this regard.

Membership inference attack (MIA) is widely deployed for auditing neural network’s privacy risks [54, 8], but state-of-the-art MIAs require loss information of models. Based on the idea that MIA is related to the model’s ability to memorize training data, we apply identity (ID) similarity to quantify the amount of information leakage of our approach. First, we measure the ID similarity between the original image data and the masked images to evaluate the privacy-preserving effect of masking. Second, we determine the similarity between the original images and the image data generated by the pre-trained model. A higher degree of similarity signifies a greater extent of information leakage. Specifically, we use CelebA-HQ 256×256 to form the masked input and pre-train a MaskDM model. The ID similarity is represented as the cosine distance between features extracted by a face recognition model[15]. More justifications for our experiment settings are provided in Appendix D.3.

In the first experiment, we implement an intuitive pipeline that randomly masks 90% image area and reconstructs the image with a masked autoencoder (MAE)[25]. We repeatedly generate a total of 10 variants for every image in the dataset. Subsequently, we evaluate on the image pairs consisting of a reconstructed image and its original counterpart. In our second experiment, we sample 3k images from the pre-trained MaskDM model and measure similarity on all possible image pairs composed of the generated images and images in the dataset. For each reference image that is either the original image in the first experiment or generated sample in the second one, we collect the maximum similarities measured on image pairs built with it. We display the probability density function (PDF) of the results in our two experiments in Fig 5. For comparison, we also measure the ID similarity on image pairs that each comprises two images sampled from the same identity in VggFace2. The resulting average ID similarity is 0.73, indicating the score level of confident identity matching. We draw the value in a green dashed line for reference.

As shown in Fig 5, in both experiments, only a small proportion of values exceed the reference line at 0.73, demonstrating that both masked images and samples generated by the pre-trained MaskDM model only contain coarse ID information from the training images. Furthermore, the PDF’s (blue curve in Fig.5) concentration around 0.6 suggests that, without additional restrictions, a substantial amount of general ID information could potentially be exposed from the training set (see visualizations in our Appendix D.2). We argue that this issue can be mitigated by implementing strict controls on sampling training samples, such as optimizing mask strategies or limiting the number of times an image can be sampled during training. The comprehensive investigation of privacy-preserving policies will be addressed in our future work.

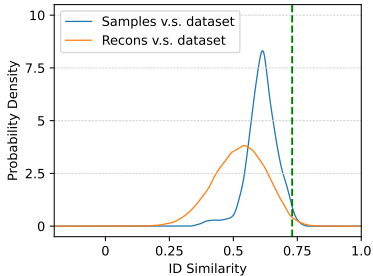


Figure 5: Density of ID similarities

5 Related Work

Efficient Training methods have drawn significant attention in generative modeling [11, 19, 12, 59, 29], and there is an urgent need for their application in the realm of diffusion models. The considerable training costs associated with diffusion models present an obstacle to entry and impede the advancement of the research community. To tackle this challenge, [48] proposes a novel approach that trains diffusion models in a low-dimensional latent space, thereby alleviating the burden on diffusion models to approximate extraneous details inherent in high-dimensional data. Another approach called MDT [20] employs masking in the training process of latent diffusion models. This method demonstrates improved efficiency based on the architecture proposed in DiT [6] for ImageNet 256×256 . However, MDT [20] is a one-stage training scheme exclusively designed for latent space training and could not benefit diffusion models trained in diverse settings. A concurrent but independent work proposes a similar approach, called patch diffusion [64], which masks the input image via cropping and trains the diffusion model following a stochastic masking schedule based on U-Net architecture. The method can be seen as a specialized instance of our method, where the architecture is CNN-based U-Net, and the mask type is chosen as cropping. Furthermore, our method could achieve significant training acceleration on CelebA-HQ 256×256 beyond the latent space compared to patch diffusion.

Vision Transformer (ViT) has revolutionized the field of various vision-related tasks. Recent research studies, such as [4, 42, 6], have incorporated ViT into diffusion model training by substituting the

prevalent CNN-based U-Net with more versatile ViT variants. These studies have empirically analyzed the factors that affect the quality of samples generated by ViT and proposed different strategies to address the challenges encountered in training ViT-based diffusion models.

Nonetheless, the predominant challenge in ViT-based diffusion models is the substantial computational burden, which includes high CUDA memory usage and lengthy training times. To mitigate these issues, ViT-based diffusion models are typically trained within the latent space (described in the Efficient Training part), given a high-dimensional data distribution (e.g., images $\geq 256 \times 256$). In this work, we propose masked denoising score matching, which, for the first time, facilitates the training of ViT-based diffusion models on data beyond the latent space while preserving manageable computational expenses.

Pre-training plays a crucial role in visual discriminative tasks [47, 36, 25, 10] and has been widely studied. It is feasible to obtain a task-specific model by relying on a pre-trained model that is optimized with a surrogate objective, such as contrastive learning [23, 14, 26] or masked image modeling [25], which facilitates exceptional generalization capabilities. However, this two-stage training paradigm has received limited attention in the image generation domain. In this regard, we introduce the successful pre-train and fine-tune framework into denoising training, termed prior-based denoising training. Furthermore, we proposed masked denoising score matching as the pre-training objective, which allows for acquiring an initial model that serves as a reasonable starting point for a wide range of downstream tasks in generative modeling.

6 Limitations

Our proposed method successfully augments the training efficiency of diffusion models and exhibits privacy-preserving capabilities, but there are some limitations. First, due to limited computing resources, we have not explored the method’s generalization across other denoising training paradigms besides DDPM. Moreover, while assessing the privacy-preserving performance of our method, we did not enforce stringent restrictions on mask sampling. Although we have demonstrated the privacy-preserving attributes of our method, a more extensive investigation into the impact factors, including masking strategies and data sampling regularities, on privacy preservation is required. With further optimization, our training framework could potentially evolve into a standard for training privacy-preserving diffusion models. We leave relevant investigations for future work.

7 Conclusion

This paper introduces prior-based diffusion training, a novel two-stage training framework that integrates pre-training into the diffusion training process for image generation models. Our approach substantially reduces the training cost while maintaining high image quality. Moreover, the framework’s first stage produces a surrogate model with strong generalization capabilities, enabling a wide range of downstream tasks. Applicable to all model architectures, including CNN and vision transformers, our training framework operates effectively beyond the latent space.

In the first pre-training stage, we propose masked denoising score matching as the optimization objective and provide an intuitive theoretical foundation explaining the advantages of incorporating prior learning into the complete training process. We then empirically investigate various masking strategies to determine the optimal settings. To demonstrate our method’s effectiveness, we conduct unconditional image synthesis using UViT in the pixel space, achieving capabilities better than a standard DDPM model while reducing training costs by 75%. In addition, we conduct experiments in realistic settings featuring distribution shifts and restricted data availability during fine-tuning to verify the generalizability of masked pre-training. The results demonstrate a notable improvement in the FID score. It is anticipated that our approach can be extended to various fields with diverse data modalities. Furthermore, we explore the privacy preserving capabilities of our masked pre-training method. Finally, we acknowledge the potential for a more appropriate pre-training objective to further improve the training of diffusion models, and we leave this exploration for our future work.

References

- [1] Martin Arjovsky, Soumith Chintala, and Léon Bottou. Wasserstein generative adversarial networks. In *International conference on machine learning*, pages 214–223. PMLR, 2017.
- [2] Omri Avrahami, Ohad Fried, and Dani Lischinski. Blended latent diffusion. *arXiv preprint arXiv:2206.02779*, 2022.
- [3] Yogesh Balaji, Seungjun Nah, Xun Huang, Arash Vahdat, Jiaming Song, Karsten Kreis, Miika Aittala, Timo Aila, Samuli Laine, Bryan Catanzaro, et al. ediffi: Text-to-image diffusion models with an ensemble of expert denoisers. *arXiv preprint arXiv:2211.01324*, 2022.
- [4] Fan Bao, Chongxuan Li, Yue Cao, and Jun Zhu. All are worth words: a vit backbone for score-based diffusion models. *arXiv preprint arXiv:2209.12152*, 2022.
- [5] Andreas Blattmann, Robin Rombach, Huan Ling, Tim Dockhorn, Seung Wook Kim, Sanja Fidler, and Karsten Kreis. Align your latents: High-resolution video synthesis with latent diffusion models. In *Proceedings of the IEEE/CVF Conference on Computer Vision and Pattern Recognition*, pages 22563–22575, 2023.
- [6] He Cao, Jianan Wang, Tianhe Ren, Xianbiao Qi, Yihao Chen, Yuan Yao, and Lei Zhang. Exploring vision transformers as diffusion learners. *arXiv preprint arXiv:2212.13771*, 2022.
- [7] Qiong Cao, Li Shen, Weidi Xie, Omkar M Parkhi, and Andrew Zisserman. Vggface2: A dataset for recognising faces across pose and age. In *2018 13th IEEE international conference on automatic face & gesture recognition (FG 2018)*, pages 67–74. IEEE, 2018.
- [8] Nicholas Carlini, Steve Chien, Milad Nasr, Shuang Song, Andreas Terzis, and Florian Tramèr. Membership inference attacks from first principles. In *2022 IEEE Symposium on Security and Privacy (SP)*, pages 1897–1914. IEEE, 2022.
- [9] Nicholas Carlini, Jamie Hayes, Milad Nasr, Matthew Jagielski, Vikash Sehwal, Florian Tramèr, Borja Balle, Daphne Ippolito, and Eric Wallace. Extracting training data from diffusion models. In *To appear in the 32nd USENIX Security Symposium*. USENIX, 2023.
- [10] Mathilde Caron, Hugo Touvron, Ishan Misra, Hervé Jégou, Julien Mairal, Piotr Bojanowski, and Armand Joulin. Emerging properties in self-supervised vision transformers. In *Proceedings of the IEEE/CVF international conference on computer vision*, pages 9650–9660, 2021.
- [11] Huiwen Chang, Han Zhang, Jarred Barber, AJ Maschinot, Jose Lezama, Lu Jiang, Ming-Hsuan Yang, Kevin Murphy, William T Freeman, Michael Rubinstein, et al. Muse: Text-to-image generation via masked generative transformers. *arXiv preprint arXiv:2301.00704*, 2023.
- [12] Huiwen Chang, Han Zhang, Lu Jiang, Ce Liu, and William T Freeman. Maskgit: Masked generative image transformer. In *Proceedings of the IEEE/CVF Conference on Computer Vision and Pattern Recognition*, pages 11315–11325, 2022.
- [13] Minghao Chen, Iro Laina, and Andrea Vedaldi. Training-free layout control with cross-attention guidance. *arXiv preprint arXiv:2304.03373*, 2023.
- [14] Xinlei Chen, Haoqi Fan, Ross Girshick, and Kaiming He. Improved baselines with momentum contrastive learning. *arXiv preprint arXiv:2003.04297*, 2020.
- [15] Jiankang Deng, Jia Guo, Niannan Xue, and Stefanos Zafeiriou. Arcface: Additive angular margin loss for deep face recognition. In *Proceedings of the IEEE/CVF conference on computer vision and pattern recognition*, pages 4690–4699, 2019.
- [16] Prafulla Dhariwal and Alexander Nichol. Diffusion models beat gans on image synthesis. *Advances in Neural Information Processing Systems*, 34:8780–8794, 2021.
- [17] Alexey Dosovitskiy, Lucas Beyer, Alexander Kolesnikov, Dirk Weissenborn, Xiaohua Zhai, Thomas Unterthiner, Mostafa Dehghani, Matthias Minderer, Georg Heigold, Sylvain Gelly, et al. An image is worth 16x16 words: Transformers for image recognition at scale. *arXiv preprint arXiv:2010.11929*, 2020.
- [18] Dave Epstein, Allan Jabri, Ben Poole, Alexei A Efros, and Aleksander Holynski. Diffusion self-guidance for controllable image generation. *arXiv preprint arXiv:2306.00986*, 2023.
- [19] Patrick Esser, Robin Rombach, and Bjorn Ommer. Taming transformers for high-resolution image synthesis. In *Proceedings of the IEEE/CVF conference on computer vision and pattern recognition*, pages 12873–12883, 2021.

- [20] Shanghua Gao, Pan Zhou, Ming-Ming Cheng, and Shuicheng Yan. Masked diffusion transformer is a strong image synthesizer. *arXiv preprint arXiv:2303.14389*, 2023.
- [21] Vidit Goel, Elia Peruzzo, Yifan Jiang, DeJia Xu, Nicu Sebe, Trevor Darrell, Zhangyang Wang, and Humphrey Shi. Pair-diffusion: Object-level image editing with structure-and-appearance paired diffusion models. *arXiv preprint arXiv:2303.17546*, 2023.
- [22] Ian Goodfellow, Jean Pouget-Abadie, Mehdi Mirza, Bing Xu, David Warde-Farley, Sherjil Ozair, Aaron Courville, and Yoshua Bengio. Generative adversarial nets. In Z. Ghahramani, M. Welling, C. Cortes, N. Lawrence, and K.Q. Weinberger, editors, *Advances in Neural Information Processing Systems*, volume 27. Curran Associates, Inc., 2014.
- [23] Jean-Bastien Grill, Florian Strub, Florent Altché, Corentin Tallec, Pierre Richemond, Elena Buchatskaya, Carl Doersch, Bernardo Avila Pires, Zhaohan Guo, Mohammad Gheshlaghi Azar, et al. Bootstrap your own latent—a new approach to self-supervised learning. *Advances in neural information processing systems*, 33:21271–21284, 2020.
- [24] Ishaan Gulrajani, Faruk Ahmed, Martin Arjovsky, Vincent Dumoulin, and Aaron C Courville. Improved training of wasserstein gans. *Advances in neural information processing systems*, 30, 2017.
- [25] Kaiming He, Xinlei Chen, Saining Xie, Yanghao Li, Piotr Dollár, and Ross Girshick. Masked autoencoders are scalable vision learners. In *Proceedings of the IEEE/CVF Conference on Computer Vision and Pattern Recognition*, pages 16000–16009, 2022.
- [26] Kaiming He, Haoqi Fan, Yuxin Wu, Saining Xie, and Ross Girshick. Momentum contrast for unsupervised visual representation learning. In *Proceedings of the IEEE/CVF conference on computer vision and pattern recognition*, pages 9729–9738, 2020.
- [27] Martin Heusel, Hubert Ramsauer, Thomas Unterthiner, Bernhard Nessler, and Sepp Hochreiter. Gans trained by a two time-scale update rule converge to a local nash equilibrium. *Advances in neural information processing systems*, 30, 2017.
- [28] Jonathan Ho, Ajay Jain, and Pieter Abbeel. Denoising diffusion probabilistic models. *Advances in Neural Information Processing Systems*, 33:6840–6851, 2020.
- [29] Jonathan Ho, Chitwan Saharia, William Chan, David J Fleet, Mohammad Norouzi, and Tim Salimans. Cascaded diffusion models for high fidelity image generation. *J. Mach. Learn. Res.*, 23(47):1–33, 2022.
- [30] Jonathan Ho, Tim Salimans, Alexey Gritsenko, William Chan, Mohammad Norouzi, and David J Fleet. Video diffusion models. *arXiv preprint arXiv:2204.03458*, 2022.
- [31] Emiel Hoogeboom, Jonathan Heek, and Tim Salimans. simple diffusion: End-to-end diffusion for high resolution images. *arXiv preprint arXiv:2301.11093*, 2023.
- [32] Phillip Isola, Jun-Yan Zhu, Tinghui Zhou, and Alexei A Efros. Image-to-image translation with conditional adversarial networks. In *Proceedings of the IEEE conference on computer vision and pattern recognition*, pages 1125–1134, 2017.
- [33] Yifan Jiang, Shiyu Chang, and Zhangyang Wang. Transgan: Two pure transformers can make one strong gan, and that can scale up. *Advances in Neural Information Processing Systems*, 34:14745–14758, 2021.
- [34] Tero Karras, Timo Aila, Samuli Laine, and Jaakko Lehtinen. Progressive growing of gans for improved quality, stability, and variation. *arXiv preprint arXiv:1710.10196*, 2017.
- [35] Tero Karras, Miika Aittala, Timo Aila, and Samuli Laine. Elucidating the design space of diffusion-based generative models. *arXiv preprint arXiv:2206.00364*, 2022.
- [36] Alexander Kirillov, Eric Mintun, Nikhila Ravi, Hanzi Mao, Chloe Rolland, Laura Gustafson, Tete Xiao, Spencer Whitehead, Alexander C Berg, Wan-Yen Lo, et al. Segment anything. *arXiv preprint arXiv:2304.02643*, 2023.
- [37] Haohe Liu, Zehua Chen, Yi Yuan, Xinhao Mei, Xubo Liu, Danilo Mandic, Wenwu Wang, and Mark D Plumbley. Audioldm: Text-to-audio generation with latent diffusion models. *arXiv preprint arXiv:2301.12503*, 2023.
- [38] Ze Liu, Yutong Lin, Yue Cao, Han Hu, Yixuan Wei, Zheng Zhang, Stephen Lin, and Baining Guo. Swin transformer: Hierarchical vision transformer using shifted windows. In *Proceedings of the IEEE/CVF international conference on computer vision*, pages 10012–10022, 2021.

- [39] Ziwei Liu, Ping Luo, Xiaogang Wang, and Xiaoou Tang. Deep learning face attributes in the wild. In *Proceedings of International Conference on Computer Vision (ICCV)*, December 2015.
- [40] Alexander Quinn Nichol and Prafulla Dhariwal. Improved denoising diffusion probabilistic models. In *International Conference on Machine Learning*, pages 8162–8171. PMLR, 2021.
- [41] Kushagra Pandey, Avideep Mukherjee, Piyush Rai, and Abhishek Kumar. Diffusevae: Efficient, controllable and high-fidelity generation from low-dimensional latents. *arXiv preprint arXiv:2201.00308*, 2022.
- [42] William Peebles and Saining Xie. Scalable diffusion models with transformers. *arXiv preprint arXiv:2212.09748*, 2022.
- [43] Hao Phung, Quan Dao, and Anh Tran. Wavelet diffusion models are fast and scalable image generators. In *Proceedings of the IEEE/CVF Conference on Computer Vision and Pattern Recognition*, pages 10199–10208, 2023.
- [44] Zeju Qiu, Weiyang Liu, Haiwen Feng, Yuxuan Xue, Yao Feng, Zhen Liu, Dan Zhang, Adrian Weller, and Bernhard Schölkopf. Controlling text-to-image diffusion by orthogonal finetuning. *arXiv preprint arXiv:2306.07280*, 2023.
- [45] Aditya Ramesh, Prafulla Dhariwal, Alex Nichol, Casey Chu, and Mark Chen. Hierarchical text-conditional image generation with clip latents. *arXiv preprint arXiv:2204.06125*, 2022.
- [46] Aditya Ramesh, Mikhail Pavlov, Gabriel Goh, Scott Gray, Chelsea Voss, Alec Radford, Mark Chen, and Ilya Sutskever. Zero-shot text-to-image generation. In *International Conference on Machine Learning*, pages 8821–8831. PMLR, 2021.
- [47] Shaoqing Ren, Kaiming He, Ross Girshick, and Jian Sun. Faster r-cnn: Towards real-time object detection with region proposal networks. *Advances in neural information processing systems*, 28, 2015.
- [48] Robin Rombach, Andreas Blattmann, Dominik Lorenz, Patrick Esser, and Björn Ommer. High-resolution image synthesis with latent diffusion models. In *Proceedings of the IEEE/CVF Conference on Computer Vision and Pattern Recognition*, pages 10684–10695, 2022.
- [49] Olaf Ronneberger, Philipp Fischer, and Thomas Brox. U-net: Convolutional networks for biomedical image segmentation. In *International Conference on Medical image computing and computer-assisted intervention*, pages 234–241. Springer, 2015.
- [50] Nataniel Ruiz, Yuanzhen Li, Varun Jampani, Yael Pritch, Michael Rubinstein, and Kfir Aberman. Dreambooth: Fine tuning text-to-image diffusion models for subject-driven generation. In *Proceedings of the IEEE/CVF Conference on Computer Vision and Pattern Recognition*, pages 22500–22510, 2023.
- [51] Chitwan Saharia, William Chan, Huiwen Chang, Chris Lee, Jonathan Ho, Tim Salimans, David Fleet, and Mohammad Norouzi. Palette: Image-to-image diffusion models. In *ACM SIGGRAPH 2022 Conference Proceedings*, pages 1–10, 2022.
- [52] Chitwan Saharia, William Chan, Saurabh Saxena, Lala Li, Jay Whang, Emily L Denton, Kamyar Ghasemipour, Raphael Gontijo Lopes, Burcu Karagol Ayan, Tim Salimans, et al. Photorealistic text-to-image diffusion models with deep language understanding. *Advances in Neural Information Processing Systems*, 35:36479–36494, 2022.
- [53] Tim Salimans, Ian Goodfellow, Wojciech Zaremba, Vicki Cheung, Alec Radford, and Xi Chen. Improved techniques for training gans. *Advances in neural information processing systems*, 29, 2016.
- [54] R. Shokri, M. Stronati, C. Song, and V. Shmatikov. Membership inference attacks against machine learning models. In *2017 IEEE Symposium on Security and Privacy (SP)*, pages 3–18, Los Alamitos, CA, USA, may 2017. IEEE Computer Society.
- [55] Jaskirat Singh, Stephen Gould, and Liang Zheng. High-fidelity guided image synthesis with latent diffusion models. In *Proceedings of the IEEE/CVF Conference on Computer Vision and Pattern Recognition*, pages 5997–6006, 2023.
- [56] Jascha Sohl-Dickstein, Eric Weiss, Niru Maheswaranathan, and Surya Ganguli. Deep unsupervised learning using nonequilibrium thermodynamics. In *International Conference on Machine Learning*, pages 2256–2265. PMLR, 2015.

- [57] Gowthami Somepalli, Vasu Singla, Micah Goldblum, Jonas Geiping, and Tom Goldstein. Diffusion art or digital forgery? investigating data replication in diffusion models. In *Proceedings of the IEEE/CVF Conference on Computer Vision and Pattern Recognition*, pages 6048–6058, 2023.
- [58] Jiaming Song, Chenlin Meng, and Stefano Ermon. Denoising diffusion implicit models. *arXiv preprint arXiv:2010.02502*, 2020.
- [59] Yang Song, Prafulla Dhariwal, Mark Chen, and Ilya Sutskever. Consistency models. *arXiv preprint arXiv:2303.01469*, 2023.
- [60] Yang Song and Stefano Ermon. Generative modeling by estimating gradients of the data distribution. *Advances in neural information processing systems*, 32, 2019.
- [61] Yang Song, Jascha Sohl-Dickstein, Diederik P Kingma, Abhishek Kumar, Stefano Ermon, and Ben Poole. Score-based generative modeling through stochastic differential equations. *arXiv preprint arXiv:2011.13456*, 2020.
- [62] Arash Vahdat, Karsten Kreis, and Jan Kautz. Score-based generative modeling in latent space. *Advances in Neural Information Processing Systems*, 34:11287–11302, 2021.
- [63] Pascal Vincent. A connection between score matching and denoising autoencoders. *Neural computation*, 23(7):1661–1674, 2011.
- [64] Zhendong Wang, Yifan Jiang, Huangjie Zheng, Peihao Wang, Pengcheng He, Zhangyang Wang, Weizhu Chen, and Mingyuan Zhou. Patch diffusion: Faster and more data-efficient training of diffusion models. *arXiv preprint arXiv:2304.12526*, 2023.
- [65] Dongchao Yang, Jianwei Yu, Helin Wang, Wen Wang, Chao Weng, Yuexian Zou, and Dong Yu. Diffsound: Discrete diffusion model for text-to-sound generation. *IEEE/ACM Transactions on Audio, Speech, and Language Processing*, 2023.
- [66] Xiulong Yang, Sheng-Min Shih, Yinlin Fu, Xiaoting Zhao, and Shihao Ji. Your vit is secretly a hybrid discriminative-generative diffusion model. *arXiv preprint arXiv:2208.07791*, 2022.

A Change Log

First update

- (1) We address some typos and we rename the term "masked score matching" to "masked denoising score matching" to better convey its relationship to denoising score matching.
- (2) We include additional experiments in section 4.5 to further investigate the privacy-preserving property of the masked pre-training method.
- (3) Section 4.2 now features restructured experiments for better clarity.
- (4) We supplement our appendix with details of the experiment that explores the training instability issue occurring in the early stages of pre-training. Additionally, we have include implementation details of all experiments in the appendix.

B Model Configurations

Specifically, we utilize the U-ViT-Small setup from [4] as our MaskDM-S model, construct MaskDM-B by removing five transformer blocks from U-ViT-Mid to ensure efficient training on a single Tesla V100 GPU for one 256×256 image input, and derived our MaskDM-L model by making similar adjustments to U-ViT-Large.

Model	Depth	Dim	Heads	Params
MaskDM-S	13	512	8	44M
MaskDM-B	12	768	12	102M
MaskDM-L	16	1024	16	233M

Table 4: Details of MaskDM models

C Implementation Details

Experiment	stage	opt	lr	bs	weight dec	ema	model	hflip	mask	gradient clip	noise
section 4.2											
CelebA	pre	AdamW	1e-4	128	0.03	0.999 every 1	MaskDM-S		10%		linear
	pre	AdamW	2e-4	256	0.03	0.999 every 1	MaskDM-S		50%		linear
	pre	AdamW	2e-4	512	0.03	0.999 every 1	MaskDM-S		90%		linear
	tuning	AdamW	1e-4	128	0.03	0.999 every 1	MaskDM-S				linear
section 4.3											
CelebA-HQ (Used DWT)	pre	AdamW	1e-4	64	0.03	0.999 every 10	MaskDM-B	0.5	70% 4x4 block	1.0	cosine
	pre	AdamW	1e-4	128	0.03	0.999 every 10	MaskDM-L	0.5	70% 4x4 block	1.0	cosine
	tuning	AdamW	1e-4	32	0.03	0.999 every 10	MaskDM-B	0.5		1.0	cosine
	tuning	AdamW	5e-5	16	0.03	0.999 every 10	MaskDM-L	0.5		1.0	cosine
section 4.4											
CelebA-HQ	pre	AdamW	2e-4	256	0.03	0.999 every 1	MaskDM-S		90% 4x4 block	1.0	cosine
	10% tuning	AdamW	5e-5	64	0.03	0.999 every 1	MaskDM-S	50%		1.0	cosine
	1% tuning	AdamW	5e-5	64	0.03	0.999 every 1	MaskDM-S	50%		1.0	cosine
section 4.5											
CelebA-HQ	pre	AdamW	2e-4	256	0.03	0.999 every 1	MaskDM-B		90%	1.0	cosine

Table 5: Hyper-parameters of experiments used during training

Lower LR used in 10% masked pre-training. In early experiments, it is observed that the model yields a poor performance when the learning rate is set to $2e-4$, using 128 batch size. Therefore, we scale the learning rate linearly according to the batch size and use $1e-4$ in our experiments.

Discrete Wavelet Transformation. When conducting unconditional image synthesis experiments on CelebA-HQ 256×256 in Sec 4.3, we incorporate Haar DWT to downsample the input image into four components: \mathbf{x}^L and $\mathbf{x}^H = (\mathbf{x}^h, \mathbf{x}^v, \mathbf{x}^{diag})$, where high-frequency components denoted as $\mathbf{x}^h, \mathbf{x}^v, \mathbf{x}^{diag}$ are concatenated along the channel dimension. The resulting spatial dimension of each component is 128×128 . We utilize separate patch embedding layers and position embeddings for \mathbf{x}^L and \mathbf{x}^H respectively.

Experiment	model	extra data	pre-train step	tuning step	sampler	# samples	FID	V100-Day
section 4.2 CelebA	Tab.1, MaskDM-S		any	any	DDIM-500, $\eta = 1.0$	1k	any	
section 4.3 CelebA-HQ (Used DWT)	Fig.4, MaskDM-L		200k	any	DDIM-250, $\eta = 0.8$	3k		
	MaskDM-L			any	DDIM-250, $\eta = 0.8$	3k		
	Tab.2, MaskDM-B		150k	550k	DDIM-500, $\eta = 0.8$	30k	10.77	2.8+24.3
	MaskDM-L		200k	550k	DDIM-500, $\eta = 0.8$	30k	9.67	10.9+23
	MaskDM-L			900k	DDIM-500, $\eta = 0.8$	30k	12.06	38.3
section 4.4 10% CelebA-HQ	Tab.3, MaskDM-S		200k	50k	DDIM-250, $\eta = 1.0$	10k	24.59	
	MaskDM-S	VggFace2	200k	50k	DDIM-250, $\eta = 1.0$	10k	20.71	
	MaskDM-S			200k	DDIM-250, $\eta = 1.0$	10k	37.17	
1% CelebA-HQ	MaskDM-S		200k	50k	DDIM-250, $\eta = 1.0$	10k	32.51	
	MaskDM-S	VggFace2	200k	50k	DDIM-250, $\eta = 1.0$	10k	36.51	
	MaskDM-S			200k	DDIM-250, $\eta = 1.0$	10k	63.33	
section 4.5 CelebA-HQ	MaskDM-B		200k		DDIM-250, $\eta = 1.0$	3k	89.21	4.9

Table 6: Sampling settings and additional information of models reported in the tables and figures of our paper

D Additional Details on Experiments

D.1 Pre-training instability

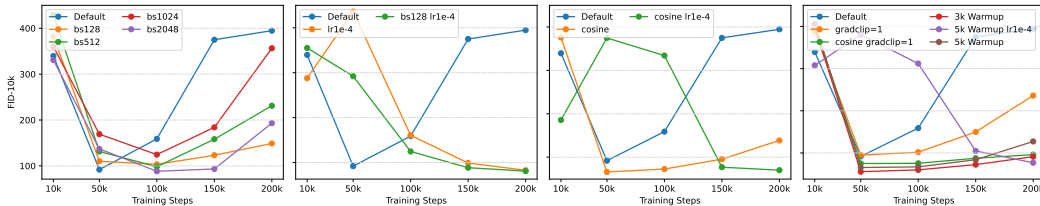


Figure 6: Experiments on the CelebA 64×64 dataset aimed at improving pre-training stability. We maintain a fixed mask ratio of 90%, while adopting the other parameters used in pre-training experiments at a 50% mask ratio (detailed in Table 5) as the default setting. Moving from left to right, we investigate the impact of various factors, including batch size, learning rate, noise schedule, gradient clipping, and learning rate schedule (Warmup). When employing Warmup, the learning rate follows a linear schedule with an initial value of $5e-5$.

In early experiments, we consistently observe that the model fails to converge when trained with a 90% mask ratio. Therefore, we study the impact of various factors on training convergence, including batch size, learning rate, noise schedule, gradient clipping and learning rate warmup. As depicted in Fig.6, increasing the batch size from 128 to 2048 still results in the model failing to converge. On the other hand, when we reduce the learning rate from $2e-4$ to $1e-4$ and decrease the batch size from 256 to 128, we observe a stable and gradual plateau in the FID score of the model after 200k training steps. However, this more conservative hyperparameter setting leads to a relatively slower convergence speed, necessitating a longer training time to achieve a similar level of performance for the model.

Subsequently, we adopt a cosine schedule in place of the linear schedule, and the resulting FID score curve demonstrates the superiority of the cosine schedule in improving the training stability of the model. It effectively mitigates the convergence issues observed with the linear schedule. Furthermore, we implement optimization tricks, such as learning rate linear schedule and gradient clipping, which also contribute to a more stable convergence of the model.

D.2 Visualizing training image-generated sample pairs

In Fig.7, Fig.8 and Fig.9, we display examples of the image pairs each composed of a training image followed by a sample generated by pre-trained MaskDM. The ID similarity of image pairs in each row is listed on the left.

ID similarity



Figure 7: Pairs of training image and generated sample

ID similarity



Figure 8: Pairs of training image and generated sample



Figure 9: Pairs of training image and generated sample

D.3 Privacy preserving

Our masked pre-training approach, which employs a high mask rate of up to 90%, offers natural advantages for privacy protection. Image diffusion models, such as DALL-E 2, Stable Diffusion, and Midjourney, are trained with large amount of data and part of the data is scraped online. Their memorization and regeneration of the training data will cause privacy-violating risks, such as infringement of copyright, violation of personal portrait right, and medical data leakage. Unfortunately, recent studies [9, 57] have demonstrated that diffusion models, less private compared with GANs, tend to memorize individual images from training data and emit them during sampling.

We consider two practical scenarios: 1) a data owner would like to provide data and pay a third party for model training but would like to protect privacy of the data; 2) a model owner would like to publish or sell the pre-trained model for third parties to use but wants to prevent privacy attacks that leak training data.

An attacker’s ultimate goal is to extract sensitive information of the training data. and the foundation of such advanced privacy attacks is the feasibility of membership inference [54, 8], which aims to determine if a sample belongs to the training dataset of a particular model. In our second scenario, the pre-trained model is a black-box to the attacker, where the loss of the model is inaccessible. Consequently, state-of-the-art membership inference attacks cannot be exploited. According to Carlini et al. [8], the capability of membership inference is related to model’s ability of memorizing data points. Therefore, In sec. 4.5, we design an intuitive strategy to evaluate the degree of privacy information leaked from the masked input data and our pre-trained model.

E Relation to denoising score matching

Denoising Score Matching, introduced by [63], is an optimization objective aimed at minimizing the expected squared distance between the predictions of a parameterized model and the score of the joint distribution $p(\mathbf{x}, \tilde{\mathbf{x}})$. Here, \mathbf{x} represents clean data, and $\tilde{\mathbf{x}}$ represents corrupted data. The score is defined as the derivatives of the log-density function w.r.t the data (e.g. $\nabla_{\tilde{\mathbf{x}}} \log p(\mathbf{x}, \tilde{\mathbf{x}})$). The objective function can be formulated as follows:

$$J_{DSM}(\theta) = \mathbb{E}_{p(\mathbf{x}, \tilde{\mathbf{x}})} \left[\frac{1}{2} \left\| \Phi_{\theta}(\tilde{\mathbf{x}}) - \frac{\partial \log p(\tilde{\mathbf{x}}|\mathbf{x})}{\partial \tilde{\mathbf{x}}} \right\|^2 \right] \quad (6)$$

In the equation, $\Phi_\theta(\tilde{\mathbf{x}})$ denotes the model parameterized by θ , which takes corrupted data $\tilde{\mathbf{x}}$ as input. In the context of DDPM, the denoising score matching objective is applied across multiple noise scales indexed by i . In our specific scenario, we introduce a slight modification through variable substitution:

$$L_{MDSM} = \sum_{i=1}^N (1 - \alpha_i) \mathbb{E}_{p_{data}(\mathbf{x}')} \mathbb{E}_{p_{\alpha_i}(\tilde{\mathbf{x}}|\mathbf{x}')} \left[\left\| \Phi_\theta(\tilde{\mathbf{x}}) - \frac{\partial \log p_{\alpha_i}(\tilde{\mathbf{x}}|\mathbf{x}')}{\partial \tilde{\mathbf{x}}} \right\|^2 \right] \quad (7)$$

Here, $\epsilon_\theta(\tilde{\mathbf{x}}) = -\sqrt{1 - \alpha_i} \Phi_\theta(\tilde{\mathbf{x}})$ and $p_{\alpha_i}(\tilde{\mathbf{x}}|\mathbf{x}') = \mathcal{N}(\tilde{\mathbf{x}}; \sqrt{\alpha_i} \mathbf{x}', (1 - \alpha_i) \mathbf{I})$. Additionally, the clean data \mathbf{x} is replaced with its visible part \mathbf{x}' , which is obtained through a masking operation.

F Additional Samples



Figure 10: Comparison of generated samples between DDPM and our model. The first and third rows showcase samples generated by DDPM models trained for 50k steps and 200k steps, respectively. The second and fourth rows display samples generated by our pre-trained models trained for the same steps. The last row displays samples generated by our model, fine-tuned for 10k steps after pre-training for 200k steps.

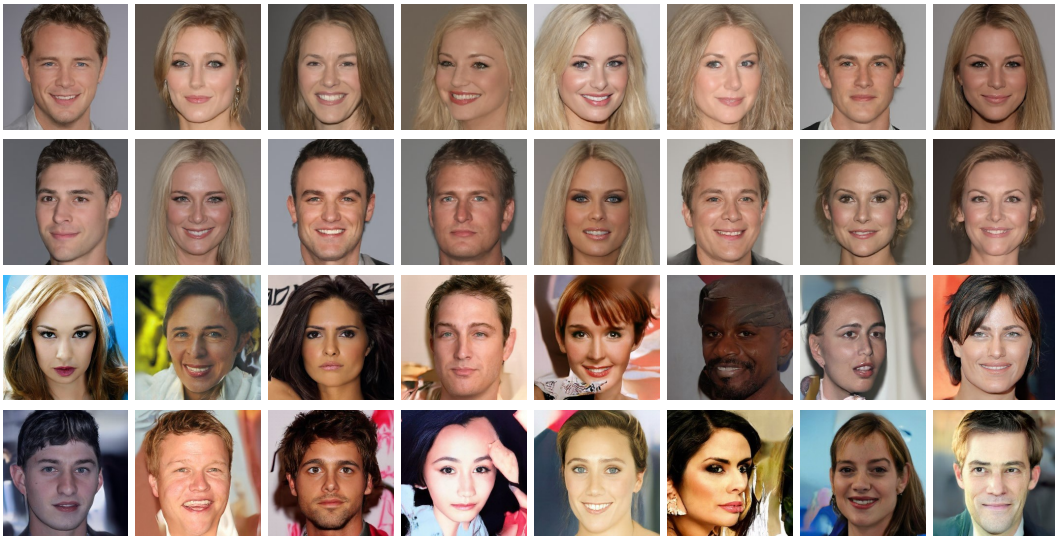


Figure 11: Uncurated samples from our MaskDM-L model reported in Tab.2. The first two rows contain samples generated by the model after 200k steps pre-training at a mask ratio of 70%. The third and fourth rows contain samples generated by the model after 550k steps fine-tuning.



Figure 12: Uncurated samples from models pre-trained with 90% 4×4 Block-wise masking. The first two rows: VGGFace2 256×256 Pre-trained model. The third and fourth rows: CelebA-HQ 256×256 pre-trained model.



Figure 13: Uncurated samples from models pre-trained on ImageNet-1K categories for 200k steps, using 90% Patch-wise masking (256×256). First and second row: samples from the class n03788365 and from model pre-trained on it. Third and fourth row: samples from the class n01729322 and from model pre-trained on it.